

SCIENTIFIC REPORTS



OPEN

New Antimicrobial Potential and Structural Properties of PAFB: A Cationic, Cysteine-Rich Protein from *Penicillium chrysogenum* Q176

Anna Huber¹, Dorottya Hajdu², Doris Bratschun-Khan¹, Zoltán Gáspári³, Mihayl Varbanov⁴, Stéphanie Philippot⁴, Ádám Fizil², András Czajlik², Zoltán Kele⁵, Christoph Sonderegger¹, László Galgóczy^{1,6}, Andrea Bodor⁷, Florentine Marx¹  & Gyula Batta²

Small, cysteine-rich and cationic proteins with antimicrobial activity are produced by diverse organisms of all kingdoms and represent promising molecules for drug development. The ancestor of all industrial penicillin producing strains, the ascomycete *Penicillium chrysogenum* Q176, secretes the extensively studied antifungal protein PAF. However, the genome of this strain harbours at least two more genes that code for other small, cysteine-rich and cationic proteins with potential antifungal activity. In this study, we characterized the *paFB* gene product that shows high similarity to PgAFP from *P. chrysogenum* R42C. Although abundant and timely regulated *paFB* gene transcripts were detected, we could not identify PAFB in the culture broth of *P. chrysogenum* Q176. Therefore, we applied a *P. chrysogenum*-based expression system to produce sufficient amounts of recombinant PAFB to address unanswered questions concerning the structure and antimicrobial function. Nuclear magnetic resonance (NMR)-based analyses revealed a compact β -folded structure, comprising five β -strands connected by four solvent exposed and flexible loops and an "abcabc" disulphide bond pattern. We identified PAFB as an inhibitor of growth of human pathogenic moulds and yeasts. Furthermore, we document for the first time an anti-viral activity for two members of the small, cysteine-rich and cationic protein group from ascomycetes.

The increasing incidence of fatal microbial infections due to the development of resistance against licensed antimicrobial drugs raises a strong demand for new antimicrobial treatment strategies. Filamentous ascomycetes are a rich source of antimicrobial bio-molecules that have the potential for wide application in medicine and agriculture to prevent and treat microbial infections¹. As such, the industrially relevant fungus *Penicillium chrysogenum* is not only a well-known producer of the β -lactam antibiotic penicillin, but also secretes small, cysteine-rich and cationic proteins with antimicrobial activity. *P. chrysogenum* is an ideal producer of bio-products with beneficial potential to mankind as it is fermentable and bulk production is easy and cheap². Most importantly, it is recognized as a "safe organism" by the US Food and Drug Administration.

The *P. chrysogenum* strain Q176 is the ancestor of all industrial strains used for penicillin production today^{2,3} and of the strains Wisconsin 54-1255⁴ and P2niaD18⁵, whose genomes were sequenced and are publicly available. *P. chrysogenum* Q176 secretes the antifungal protein PAF whose structural and functional properties have been extensively studied⁶⁻⁸. PAF represents a promising bio-molecule for novel antifungal drug development as

¹Division of Molecular Biology, Biocenter, Medical University of Innsbruck, Innrain 80-82, 6020, Innsbruck, Austria.

²Department of Organic Chemistry, Faculty of Science and Technology, University of Debrecen, Egyetem tér 1, 4032, Debrecen, Hungary. ³Faculty of Information Technology and Bionics, Pázmány Péter Catholic University, Práter u. 50A, 1083, Budapest, Hungary. ⁴SRSMC, UMR 7565, Université de Lorraine - CNRS, Faculté de Pharmacie, 5 rue Albert Lebrun, BP 80402, 54001, Nancy, France. ⁵Department of Medical Chemistry, Faculty of Medicine, University of Szeged, Dom Sq 8, 6720, Szeged, Hungary. ⁶Department of Microbiology, Faculty of Science and Informatics, University of Szeged, Közép fasor 52, 6726, Szeged, Hungary. ⁷Institute of Chemistry, Laboratory of Structural Chemistry and Biology, Eötvös Loránd University, Pázmány Péter sétány 1/A, 1117, Budapest, Hungary. Anna Huber and Dorottya Hajdu contributed equally to this work. Correspondence and requests for materials should be addressed to F.M. (email: florentine.marx@i-med.ac.at) or G.B. (email: batta@unideb.hu)

it is stable against proteolytic degradation, thermo-resistant and active within a broad pH range⁹, and shows no cytotoxic effects *in vitro*¹⁰ or *in vivo*^{11,12}. Furthermore, PAF could serve as a potential bio-pesticide in agriculture to impede infection by plant-pathogenic fungi¹³.

Genome mining in the strain Wisconsin 54-1255 for nucleotide (nt) sequences coding for other small, cysteine-rich and cationic proteins revealed that this *P. chrysogenum* strain harbours - apart from the *paf* gene (NCBI accession no. Pc24g00380)¹⁴ - two more genes that code for proteins with potential antimicrobial activity: Pc21g12970 and Pc12g08290. The product of the first gene (NCBI accession no. XP_002568323) is identical to the Pc-Arctin isolated from the arctic *P. chrysogenum* strain A096¹⁵, which represents an orthologue of the “bubble protein” isolated from the exudate of *Penicillium brevicompactum*^{15,16}. The product of the second gene (GeneBank accession no. CAP80456) is orthologous to PgAFP identified in the supernatant of *P. chrysogenum* strain RP42C, originally isolated from dry-cured ham by Rodríguez-Martín *et al.*¹⁷. Thus, the genome of *P. chrysogenum* Wisconsin 54-1255 and its progenitor strain Q176 contain at least three genes that code for proteins with reported antifungal activity. This represents a unique chance to investigate their function within one organism.

PAF, PgAFP and Pc-Arctin have in common that they are encoded as prepro-proteins containing a signal peptide followed by a pro-sequence, both of which are removed during the protein maturation process for secretion into the culture supernatant^{14,15,17}. The mature proteins are cationic due to a high content of amino acids (aa) with positively charged side-chains. Phylogenetic analyses suggested a classification of the three proteins into different groups, whereby Pc-Arctin is grouped more distantly from PAF and PgAFP^{1,18}.

While the predicted PgAFP-orthologous protein from *P. chrysogenum* Q176 has not been isolated and characterized to date, a high thermo-, pH- and protease stability has been reported for the mature PgAFP of strain RP42. Potent growth inhibitory activity against toxigenic moulds on dry-ripened sausages renders this protein interesting for the control of unwanted food contamination¹⁹.

In the present study, we isolated and studied the PgAFP orthologous protein from *P. chrysogenum* Q176 and addressed unanswered questions concerning its 3D solution structure, antimicrobial specificity and mode of action. To distinguish between the two proteins originating from the two different *P. chrysogenum* strains Q176 and RP42 we named the protein from strain Q176 *P. chrysogenum* AntiFungal protein B (PAFB), in analogy to the nomenclature of the already extensively studied homologous protein PAF from *P. chrysogenum* Q176¹⁴. We adapted the recently described *P. chrysogenum*-based expression system²⁰ to generate sufficient amounts of PAFB for functional and structural characterization. The use of the *paf*-deficient *P. chrysogenum* Q176 strain (Δpaf) as recipient ensured optimal high yield PAFB production by avoiding co-expression of the related antifungal protein PAF. We identified a disulphide-bond stabilized and compact β -folded structure of PAFB and found - apart from a growth inhibitory activity against moulds and yeasts - anti-viral activity, which has never been reported before for any member of the small, cationic and cysteine-rich protein group from ascomycetes.

Results

The *pafB* gene transcription. Our efforts failed so far to identify PAFB in the supernatant or cell extracts of *P. chrysogenum* Q176 grown under standard conditions (shaking culture in minimal medium MM at 25 °C for up to 6 days) (Fig. 1). The same was true for the *P. chrysogenum* strain Δpaf that lacks the PAF-encoding gene²¹. We examined this mutant to increase the chance to identify PAFB in the absence of PAF (data not shown). Therefore, we performed Northern blot analyses to determine the abundance and timing of *pafB* transcription. Surprisingly, we found that *pafB* mRNA was detectable in *P. chrysogenum* Q176 shaking cultures with an expression maximum at 48 h after inoculation and a subsequent decrease in transcript amount upon further incubation time (Fig. 1a).

In contrast, gene transcripts of *paf* could be detected from 48 h after inoculation onwards and transcription reached its maximum at 72 h (Fig. 1b). This expression pattern correlated with the secretion of PAF protein into the culture broth of *P. chrysogenum* Q176 during the stationary growth phase as reported¹⁴. This result was confirmed by Western blot by using a specific anti-PAF antibody²² (Fig. 1c, Supplementary Methods).

Incorrect mRNA processing could result in defective protein translation and the production of nonsense protein products that are readily degraded^{23,24}. Therefore, we next investigated if the *pafB* mRNA was correctly spliced. The verification of the *pafB* mRNA sequence was done by cDNA synthesis, PCR amplification of the *pafB* specific transcript and subsequent Sanger sequencing. The obtained sequence matched that of the exons of the *pafB* fragment (Pc24g00380) from the *P. chrysogenum* Wisconsin 54-1255 genome¹⁴ and yielded an intact *pafB* open reading frame indicating correct splicing (Supplementary Fig. S1). Similar to the *paf* gene¹⁴, two short introns (63 nt and 62 nt in length, respectively) are present in *pafB* that contain the consensus 5'-splice donor site (GT) and the consensus 3'-splice acceptor site (AG). A consensus sequence for the internal putative lariat formation element (RCTRAC) can be found in the first intron, but not in the second non-coding sequence (Supplementary Fig. S1).

The nt sequence of the *pafB* cDNA (deposited at European Nucleotide Archive (ENA), accession no. LT854946) codes for a 92 aa protein (Supplementary Table S1). Comparison of the PAFB primary sequence with that of the orthologous PgAFP revealed that PAFB differed in three aa, resulting in 97% identity of both proteins (Fig. 2). A histidine to glutamine substitution at position 2 resides in the pre-sequence, serine to asparagine and threonine to arginine substitutions at positions 19 and 23, respectively, occur in the pro-sequence (Fig. 2a). The predicted mature PAFB protein exhibited 100% identity with the mature PgAFP (Fig. 2b). The similarity of PAFB with PAF was 43% for the prepro-proteins and 35% for the mature proteins (Fig. 2b).

Recombinant expression and purification of PAFB. As we could not detect and isolate PAFB from the *P. chrysogenum* Q176 culture supernatant, we employed the *P. chrysogenum*-based expression system²⁰ to produce recombinant PAFB for structural analysis and functional tests. To this end, the *P. chrysogenum* Δpaf strain was transformed with a *Pst*I-linearized plasmid carrying the *pafB* gene under the control of the strong *paf* promoter²⁰. Positively transformed, *ptrA*-resistant *P. chrysogenum* clones were tested for highest protein secretion

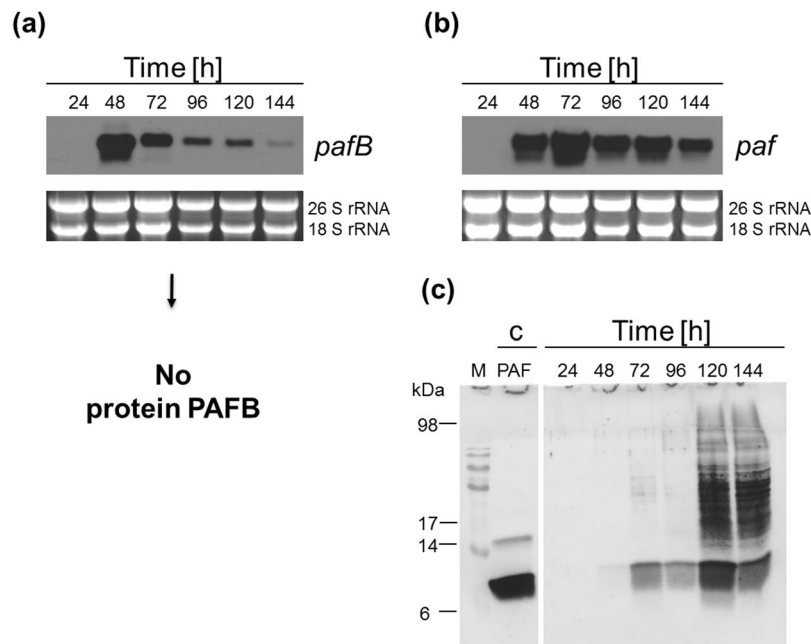


Figure 1. Expression of *pafB* and *paf* in *P. chrysogenum* Q176 submerge cultures. Samples were taken after 24, 48, 72, 96, 120 and 144 h of incubation at 25 °C. For Northern blot analysis 10 µg total RNA were loaded per lane on a 1.2% denaturing agarose gel, blotted and hybridized with a (a) *pafB* or (b) *paf* specific DIG-labelled probe. Ethidium bromide-stained 26S and 18S rRNA is shown as loading control. (c) For Western blot analysis, 25 µL of 10-fold concentrated culture supernatants were loaded per lane, size fractionated on a 18% (w/v) SDS-polyacrylamide gel and transferred on a nitrocellulose membrane. A polyclonal antibody was used for specific PAF detection. (c) purified PAF (1 µg) was loaded as a control. Gels and blots in (a), (b) and (c) were cropped for clarity. Full-length gels and blots are included in the Supplementary Information.

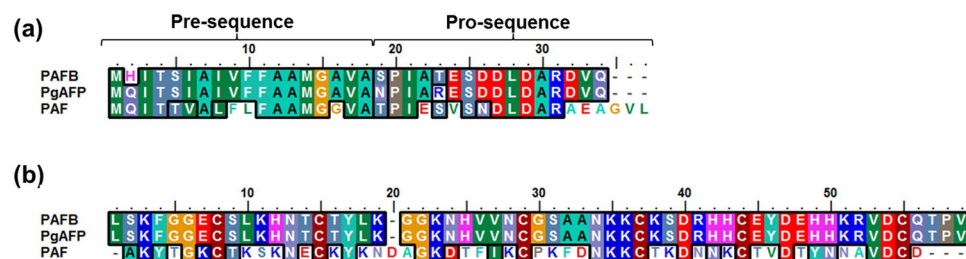


Figure 2. ClustalW alignment of the (a) prepro-sequences and (b) sequences of the mature proteins PAFB, PgAFP (UniProt ID: D0EXD3) and PAF (Uniprot ID: Q01701). Alignment was performed using the software BioEdit Sequence Alignment Editor.

over a time course of 96 h using small-scale fermentation (data not shown). Southern blot experiments with the best PAFB producer clone (*P. chrysogenum pafB*) revealed multiple random integration events of the transforming DNA into the fungal genome (Supplementary Fig. S2). This clone was selected and cultivated under large scale culture conditions.

PAFB was purified from the cell-free culture broth by a single-step chromatography. A protein yield of 61 ± 11 mg/L supernatant was reached. Purity and identity of PAFB were verified by sodium-dodecyl-sulphate polyacrylamide gel electrophoresis (SDS-PAGE) and electrospray ionization mass spectrometry (ESI-MS), respectively (Fig. 3). On the SDS-PA gels one single band for PAFB was visible in the elution fractions (Fig. 3a). ESI-MS detected one main peak corresponding to an average mass of 6.49 kDa, which represented full-length PAFB (Fig. 3b). Two smaller peaks corresponding to 6.37 kDa and 6.29 kDa correlated with two N-terminally truncated PAFB forms: the 6.37 kDa peak corresponded to a variant without the N-terminal leucine and the 6.29 kDa peak to a form that lacked the N-terminal residues leucine and serine (Fig. 3b; Supplementary Table S1). The average molecular masses of all three peaks matched the calculated theoretical molecular masses (ProtParam tool of Expasy)²⁵ of the oxidized protein forms indicating the presence of three intra-molecular disulphide bonds in all three PAFB protein variants. They all lacked any post-translational modifications, except for the cleavage of the prepro-sequence, as reported for wild-type PAF²⁰.

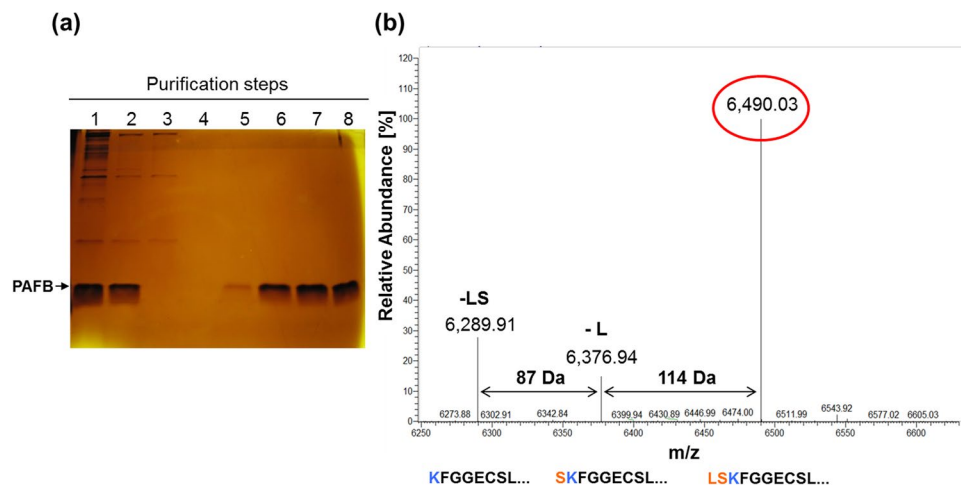


Figure 3. Verification of purified recombinant PAFB. **(a)** Samples of PAFB purification steps (25 μ L per lane) loaded on a 18% (w/v) SDS-polyacrylamide gel and silver-stained. 1, crude supernatant of 96 h-old culture; 2, ultra-filtrated culture broth (<30 kDa); 3, flow through of cation exchange chromatography; 4, column wash fraction; 5–8, elution fractions containing pure PAFB. The gel was cropped for clarity. The full-length gel is included in the Supplementary Information. **(b)** ESI-MS spectrum of purified PAFB. The x-axis represents the ratio between mass and charge and the y-axis represents the relative abundance of isotopes. The masses correspond to the different N-terminally truncated PAFB forms: the full-length (6,490.03 Da) and the two truncated variants, lacking either one (6,376.94 Da, -Leu) or two amino acids (6,289.91 Da, -Ser/-Leu), respectively. The three aa sequences below the peaks represent the N-terminus variations of recombinant PAFB.

We used the purified recombinant PAFB to generate polyclonal anti-PAFB antibodies with the aim to identify PAFB at higher specificity and sensitivity in the supernatant and cell extract of *P. chrysogenum* Q176 shaking cultures by Western blot technique (Supplementary Methods). The polyclonal anti-PAFB antibodies specifically recognized recombinant PAFB, but not PAF in Western blots (Supplementary Fig. S3). However, no PAFB-specific signals could be identified in the *P. chrysogenum* supernatants and cell extracts at the growth conditions applied, supporting our observation that PAFB was not present at concentrations that were sufficient for detection, although its encoding gene was transcribed (Supplementary Fig. S3).

NMR analysis. To obtain structural information on PAFB with atomic resolution, solution nuclear magnetic resonance (NMR) spectroscopy experiments were performed. According to the ESI-MS data, three isoforms of unlabelled PAFB were present in solution. MS peak intensities (Fig. 3) and NMR of ^{15}N -labelled PAFB suggested that the full-length PAFB sequence (58 residues) is the dominant form in the mixture. NMR spectra and MS analysis of the $^{15}\text{N}/^{13}\text{C}$ -labelled PAFB, however, identified only the shortest sequence (56 aa) (Supplementary Fig. S4). We named this short PAFB variant “short-form PAFB” (sfPAFB) and all aa sequence numbering below refers to this variant. Based on triple resonance NMR spectra, all amide H^{N} and N^{H} atoms could be found and assigned in the ^{15}N - ^1H heteronuclear single quantum correlation (HSQC) spectrum of sfPAFB (Supplementary Fig. S5) except for Lys1 because the first N-terminal residue of proteins cannot be detected in the ^{15}N -HSQC spectrum. Gly18, which resides in the middle of the big flexible loop 3, adjacent to Gly19 (Fig. 4), did not show a visible amide NH signal. However, other signals belonging to Gly18 were unambiguously assigned (CA and HA2, HA3). We note that for the ^{15}N -labelled sample, the missing Lys1 NH signals could be found. The two overlaid ^{15}N -HSQC spectra of the short ($^{15}\text{N}/^{13}\text{C}$ -labelled) and full-length (^{15}N -labelled) forms of PAFB exhibited good agreement for most of the peaks (Supplementary Fig. S5). As our structure calculations were based on measurements of the $^{15}\text{N}/^{13}\text{C}$ form, we decided to solve the structure of sfPAFB. As discussed below in more detail, there is no indication that the structures of PAFB and sfPAFB would exhibit differences except for the N-terminus.

The extent of backbone assignment (considering H^{N} , H^{C} , C^{α} and H_{α} atoms in sfPAFB) reached 94.3%, and the extent of assigned protons including side chain hydrogens was 78.1%. During the ATNOS-CANDID-Cyana run 976 nuclear Overhauser effects (NOEs) were considered in the seventh cycle which resulted in an average of 17.4 NOEs/residue. The abundant distance information compared to the size of the protein resulted in a well-defined structure with very low backbone RMSD value of the final model (0.3 Å). Chemical shift data and NMR experimental parameters were submitted to the BMRB (entry no. 26001) and the structure model of sfPAFB was deposited in the Protein Data Bank (ID: 2NC2).

The structure of sfPAFB contains two orthogonally packed triple-stranded β -pleated sheets (Fig. 4). It should be noted that there are only five strands present in the protein, because the first β -strand is shared by the sheets. They are located between residues Gly4 and Cys6, Thr12 and Leu16, Asn21 and Asn25, His40 and Asp44 as well as Arg49 and Asp51, respectively. The strands are connected by three small loops (1, 2, 4) and one large loop (3) comprising β -turn motives (Fig. 4). Finally, the two β -pleated sheets have the following β -strand pattern: β 1- β 2- β 3 and β 1- β 4- β 5, respectively. There are six highly conserved cysteines in the amino acid sequence of sfPAFB in the form of three disulphide bonds between the cysteines 6 and 34, 13 and 41 as well as 26 and 52. Note

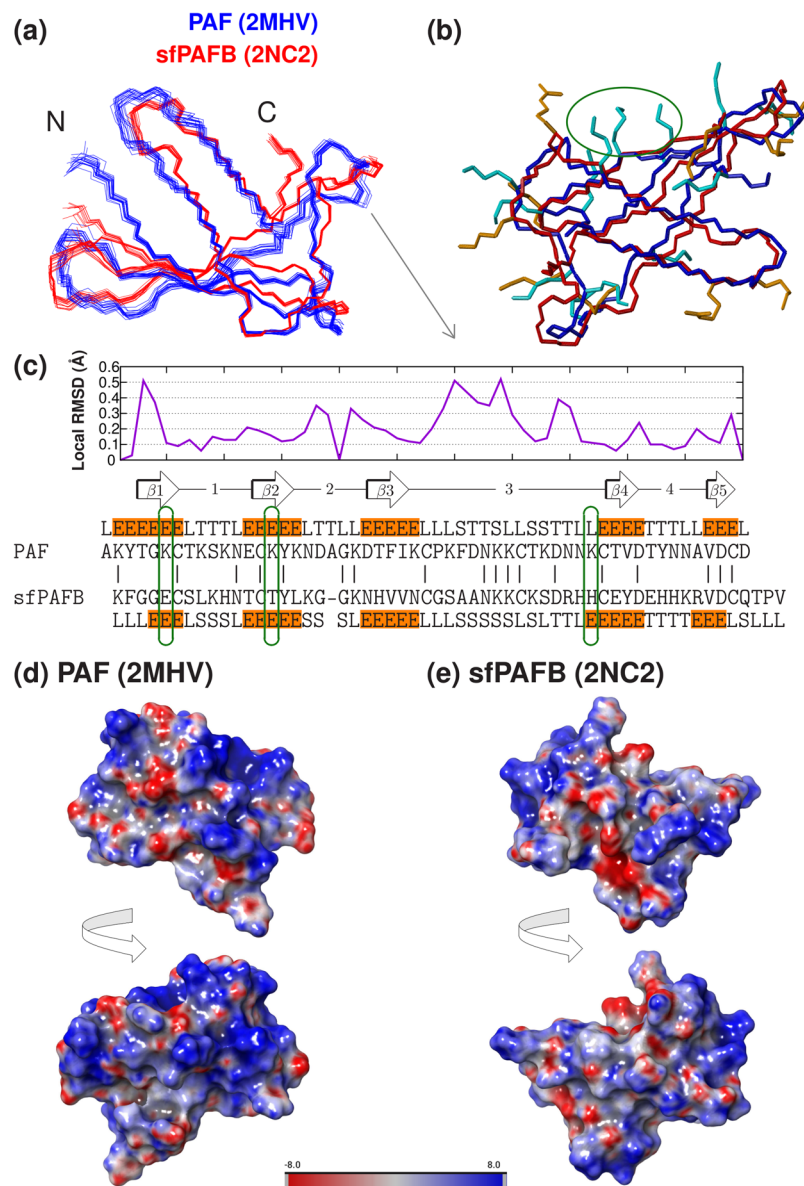


Figure 4. Comparison of the structures of sfPAFB and PAF. **(a)** Superimposed structure of sfPAFB (Protein Data Bank, ID: 2NC2, red) and PAF (Protein Data Bank, ID: 2MHV, blue). The N- and C-termini are indicated. **(b)** Superimposed structures with the lysine and arginine residues highlighted in stick representation (orange for sfPAFB and cyan for PAF). **(c)** Local RMSD calculated for the superimposed structures along the structure alignment generated with MAMMOTH-Mult. The position of the β -strands (β_1 , β_2 , β_3 , β_4 , β_5) as assigned with DSSPcont are highlighted with arrows and orange backgrounds in the DSSPcont secondary structure labels, respectively (E for Extended, T for Turn, S for Bend, L for Loop). The three lysine residues forming a ‘belt’ in PAF are circled in green and the corresponding positions in the alignment are boxed in green. The loop regions 1–4 are indicated with lines. The arrow in light grey points out the loop region with the largest local RMSD differences. **(d)** and **(e)** Electrostatic surface potential of PAF and sfPAFB, respectively, in corresponding orientations.

that this pattern (*abcabc*) creates a hidden central core region. While loops 1 and 4 form turn conformations, the secondary structure analysis showed the presence of a bend in the flexible glycine-glycine motives containing loop 2. The second and third β -strands are relatively hydrophobic compared to the other parts of the protein having no charged residues. In contrast, the central part of loop 3, the so-called large loop, contains three (32, 33 and 35) conserved lysine residues, which, together with Lys9, form a positively charged surface region. In general, the large loop adopts a bent conformation, but at its C-terminal end (Asp37-Arg38) a β -turn structure is formed. The side-chain of Asp37 is close to those of Arg38 and Lys9, respectively. Interestingly, strand β_4 in the middle of the second β -sheet exhibits high negative charge density. Nevertheless, there are several basic amino acids in its vicinity that potentially also form salt-bridges. Although both strands, β_1 and β_5 , are relatively short, several H-bonds can be found between them and strand β_4 , stabilizing the second β -sheet. The side-chains of

Organisms	MIC [μM]	
	PAFB	PAF
Filamentous fungi		
<i>A. fumigatus</i>	0.25	1
<i>A. niger</i>	0.50	0.25
<i>A. terreus</i>	1	32
<i>N. crassa</i>	0.12/0.25 [§]	0.06/0.06 [§]
<i>P. chrysogenum</i>	0.50	>32
<i>T. rubrum</i> [#]	0.5	0.25
Yeasts		
<i>C. albicans</i>	1	4
<i>S. cerevisiae</i>	1	2
Bacteria		
<i>E. coli</i>	>32	>32
<i>B. subtilis</i>	>32	>32

Table 1. Minimal inhibitory concentrations (MIC) of PAFB and PAF on fungi and bacteria. [§]0.2 \times Vogel's medium. [#]Due to slow proliferation rate the MIC of *T. rubrum* was determined after 8 days of incubation.

Tyr43 and Tyr15 interact with each other, and together with other apolar amino acids they form a hydrophobic core in sfPAFB. Finally, after the fifth, amphipathic β -strand, the C-terminal region of sfPAFB does not adopt any particular regular secondary structure.

Despite the relatively low sequence similarity (35.2%), the structure of sfPAFB is highly similar to that of PAF determined previously (Protein Data Bank ID: 2MHV). Both proteins adopt a Greek key super-secondary structure and β -barrel global fold with identical disulphide bond pattern (*abcabc*). In order to compare their local conformation, the structures of the two proteins were superimposed. Their RMSD values were below 0.5 Å overall and 0.2 Å in the β -strands (Fig. 4) except for the N-terminus. However, it turned out that the conformation of loop 3 also shows substantial differences between PAF and sfPAFB. This was unexpected because the second half of loop 3 is one of the most highly conserved regions in these proteins with the longest patch of conserved residues (asparagine-lysine-lysine-cysteine) located here (Fig. 4), whereas the β -strands generally show a lower level of sequence conservation. While both of the proteins adopt a bent structure in this region, in PAF it resulted in a turn-like conformation both at residues Asp32-Asn33 and Asp39-Asn40 amino acids, respectively. In contrast, only the latter turn is present in sfPAFB at positions Asp37-Arg38. It should also be noted that although the high density of positive surface charges is believed to be a major contributor to the activity of PAF⁸, only four lysine residues are conserved between PAF and PAFB. Furthermore, PAFB lacks a 'belt' of structurally aligned lysine residues (Lys 6, 15, 42 in PAF) and has generally lower overall positive surface charge and a different surface electrostatic potential (Fig. 4). To assess the possible differences between sfPAFB and the full-length protein, we built a first-approximation structural model of full-length PAFB by adding a leucine-serine segment to the N-terminus of the experimental sfPAFB structure. Short molecular dynamics (MD) runs suggest that the full-length N-terminus might align to strand β 4 (residues 41–45) to form an N-terminal β -strand longer than in the sfPAFB form similar to the case of PAF (Supplementary Fig. S6). This is also plausible based on the favourable interaction between Lys1 and Asp42 (sfPAFB numbering) formed during the MD calculations. Nevertheless, we do not expect that the structures of sfPAFB and full-length PAFB exhibit substantial differences. Finally, the variation of the N-terminus does not dramatically change the biophysical features of the PAFB forms, such as isoelectric point (pI), net charge and the grand average of hydropathy (GRAVY) (Supplementary Table S1).

Antifungal activity of PAFB. The growth inhibitory activity of PAFB was tested on filamentous fungi, yeasts and bacteria in 96-well microtiter plate assays by determination of the minimal inhibitory concentration (MIC) (Table 1). PAF was used as a control and for comparison. Among the filamentous fungi tested, the model organism *Neurospora crassa* showed the highest PAFB-sensitivity (MIC 0.12 μM in 0.1 \times PDB), followed by the opportunistic human pathogens *Aspergillus fumigatus* (MIC 0.25 μM), *Trichophyton rubrum* (MIC 0.5 μM), and *Aspergillus terreus* (1 μM). Interestingly, low doses of PAFB (0.5 μM) had self-inhibition activity on the producing strain *P. chrysogenum* Q176 in 0.1 \times PDB. This stands in contrast to PAF, which did not affect the germination of *P. chrysogenum* at the concentrations tested.

So far, no anti-yeast activity has been reported for PgAFP in malt extract broth¹⁹ and for PAF in YPD medium²⁶. We found, however, a clear inhibitory activity for PAFB and PAF at MICs of 1 μM and 2–4 μM on the model yeast *Saccharomyces cerevisiae* and the opportunistic human pathogen *Candida albicans*, respectively, when cultivated in 0.1 \times PDB. In contrast, no anti-bacterial activity of PAFB could be observed in the administered concentration range (0–32 μM) on the Gram-negative *Escherichia coli* and the Gram-positive *Bacillus subtilis*, which is similar to what is found for PAF.

PAFB efficiently prevented the conidial germination of all tested filamentous fungi at the respective MIC, except for *N. crassa*. Similar to previous observations with PAF²⁷, *N. crassa* conidia still germinated in the presence of PAFB, but the elongation of the germ tubes was inhibited irrespective of the culture medium applied (0.1 \times PDB or 0.2 \times Vogel's). The growth inhibitory activity of PAFB was further characterized for *N. crassa* 0.2 \times Vogel's medium, in which PAFB exhibited a comparable MIC as in 0.1 \times PDB (Table 1). *N. crassa* conidia

	Germination efficiency [%] ^{a,b}	Germ tube length [μm] ^b
control	83.30 ± 2.69	60.32 ± 10.04
PAFB	53.14 ± 5.70**	17.99 ± 2.41**
PAF	85.56 ± 1.07	48.22 ± 7.34*

Table 2. The effect of the MIC of PAFB and PAF on the colony establishment of *N. crassa*. ^aThe germination efficiency is indicated in (%) compared to the total conidial count used, which was set to be 100%. ^bThe values are given as mean ± SD (n = 3). Significant differences (p-values) between values were determined by comparison with the untreated control. *p ≤ 0.05, **p < 0.0001.

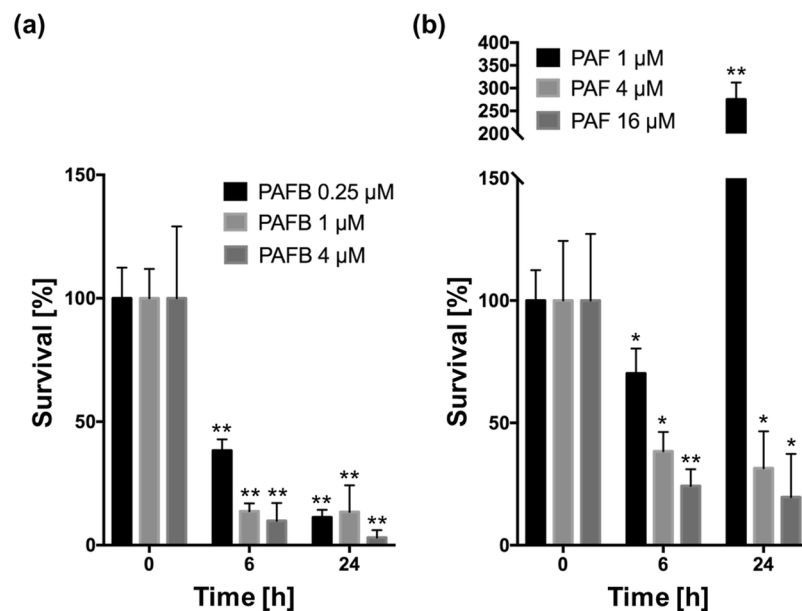


Figure 5. Antifungal effect of PAFB and PAF on *C. albicans*. Cells were exposed to 0.25 × MIC, 1 × MIC and 4 × MIC of (a) PAFB and (b) PAF. Samples at appropriate dilutions were plated on 0.1 × PDA after 0 (control), 6 and 24 h of incubation and the number of colony forming units was determined after 24 h. Colony numbers counted without incubation (0 h) were set as 100%. Values represent the mean ± SD (n = 6). Significant differences (p-values) between values were determined by comparison with the respective survival rate at 0 h. *p < 0.001, **p < 0.0001.

exposed to 0.25 μM PAFB for 6 h in 0.2 × Vogel's medium germinated at a significantly lower rate (53.14 ± 5.70%, p < 0.0001) than the untreated control (83.30 ± 2.69%) (Table 2). PAF-exposure, by contrast, did not influence the germination efficiency, as 85.56 ± 1.07% of the conidia germinated in the presence of 0.06 μM PAF compared to the untreated control (Table 2).

Furthermore, PAFB significantly reduced the germ tube length of 6 h old germlings to 17.99 ± 2.41 μm at its MIC, which corresponded to a reduction of ~70% compared to the untreated control (60.32 ± 10.04 μm, p < 0.0001). By contrast, PAF reduced the germ tube length less severely at its MIC (48.22 ± 7.34 μm; p ≤ 0.05; ~20% compared to control) (Table 2). The increase of the PAFB and PAF concentration to 2 × MIC, respectively, did not further aggravate these effects on *N. crassa* (data not shown). Thus, our findings indicated that PAFB affects colony establishment of *N. crassa* more effectively than PAF.

It is of great relevance that an antifungal drug acts fungicidal rather than fungistatic to reduce the risk of resistance development, which occurs more readily with drugs showing fungistatic activity. We therefore tested the fungicidal potential of PAFB and PAF on the wide-spread human opportunistic pathogen *C. albicans*, which causes candidiasis. To this end, *C. albicans* cells were incubated with the antifungal proteins at concentrations corresponding to 0.25–4 × MIC for 0 h (control), 6 h and 24 h in 0.1 × PDB and were then plated in appropriate dilutions onto PDA plates to allow surviving cells to establish colonies.

As shown in Fig. 5a, viability was significantly reduced after 6 h of incubation in the presence of PAFB in a dose-dependent manner. The survival rate was 38.33 ± 4.49% (p < 0.0001) at 0.25 μM, 13.74 ± 3.16% (p < 0.0001) at 1 μM and 9.81 ± 7.24% (p < 0.0001) at 4 μM compared to the viability of the respective controls (0 h of incubation) which were set to be 100%, respectively. The fungicidal potential was further increased when *C. albicans* cells were exposed to PAFB for 24 h. Compared to the survival rate of the controls (100%), only 11.24 ± 3.07% (p < 0.0001), 13.45 ± 10.79% (p < 0.0001) and 3.08 ± 2.99% (p < 0.0001) cells survived when exposed to 0.25, 1 and 4 μM, respectively (Fig. 5a).

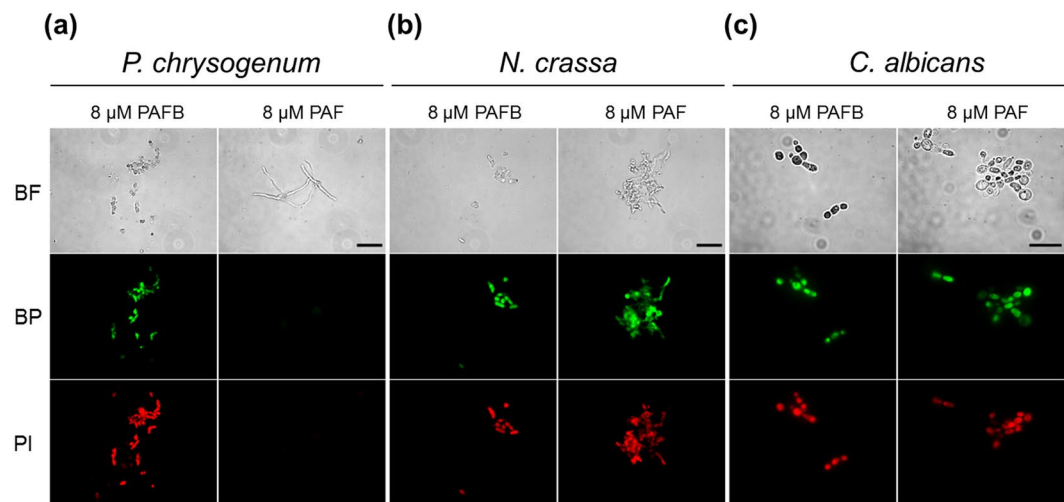


Figure 6. Uptake of BODIPY-PAFB and BODIPY-PAF in germlings of (a) *P. chrysogenum*, (b) *N. crassa* and (c) *C. albicans* cells. Samples were taken after 12 h of incubation of conidia of *P. chrysogenum* and *N. crassa* and after 6 h of incubation of *C. albicans* cells with BODIPY-labelled proteins. Co-staining with PI was applied 10 min before imaging. BF = Brightfield, BP = BODIPY-labelled proteins. Scale bars = 30 μm in (a,b), scale bar = 15 μm in (c).

Similarly, *C. albicans* cells exposed to PAF showed reduced viability after 6 h of incubation (Fig. 5b). The fungicidal effect of PAF, however, was less pronounced than that with PAFB. The survival rate was $70.21 \pm 10.17\%$ ($p < 0.001$) at 1 μM PAF, $38.35 \pm 7.92\%$ ($p < 0.001$) at 4 μM PAF and $24.21 \pm 6.88\%$ ($p < 0.0001$) at 16 μM PAF, which corresponded to $0.25 \times \text{MIC}$, $1 \times \text{MIC}$ and $4 \times \text{MIC}$, respectively, compared to the control cells (100% survival at 0 h of incubation) (Fig. 5b). This fungicidal effect was detectable with 4 μM and 16 μM PAF at longer incubation times (survival rates after 24 h: $31.48 \pm 15.05\%$ ($p < 0.001$) and $19.65 \pm 17.68\%$ ($p < 0.001$), respectively) (Fig. 5b), whereas PAF was less effective at low concentration ($0.25 \times \text{MIC}$) and with shorter incubation times (6 h). *Candida* cells exposed to 1 μM PAF proliferated further when cultivated for 24 h in liquid $0.1 \times \text{PDB}$, which became evident from the increased number of colony forming units when plated on PDA plates.

Our results indicate that PAFB acts fast and efficiently in a fungicidal way on *C. albicans* at a sub-MIC concentration.

Localization of PAFB in fungi. In previous studies, we reported that PAF toxicity in sensitive fungi is closely linked with its active internalization into the cell^{8,22}. Therefore, we examined the uptake and localization of PAFB in comparison to PAF in *N. crassa*, *P. chrysogenum* and *C. albicans*. For this purpose, PAFB and PAF were labelled with the green fluorescent dye BODIPY. Both proteins had comparable labelling efficiencies and the antifungal activity was similar to that of the unlabelled proteins (data not shown). To visualize the fluorescence signals 8 μM of protein conjugates were applied.

The conidia of *N. crassa* and *P. chrysogenum* were allowed to germinate for 12 h, the cells of *C. albicans* to grow for 6 h in the presence of BODIPY-PAFB and BODIPY-PAF, respectively, before the fungal cells were co-stained with propidium-iodide (PI) to test cell viability. As shown in Fig. 6(b,c), both BODIPY-labelled proteins localized in germlings of *N. crassa* and in *C. albicans* cells, which undoubtedly showed signs of cell death by positive PI staining. The same was observed with *P. chrysogenum* germlings, in which BODIPY-PAFB uptake correlated with PI staining. By contrast, we did neither detect BODIPY-PAF uptake nor PI staining in *P. chrysogenum* (Fig. 6a). These observations matched with the different susceptibilities of *P. chrysogenum* for PAFB and PAF described above (Table 1) and provide further evidence that antifungal toxicity of PAFB and PAF is closely linked to their uptake into fungal cells.

We further analysed the uptake mechanism of BODIPY-PAFB in *N. crassa* in time course experiments. After 30 min of incubation, BODIPY-PAFB had already attached to the envelope of *N. crassa* conidia and intracellular signals were visible (Fig. 7). With prolonged incubation time (>2 h), the PAFB signals in the cytoplasm steadily increased which coincided with positive PI staining (Fig. 7). Interestingly, fungal cells showed no signs of cell death as long as BODIPY-PAFB resided in vacuoles (Fig. 7).

We investigated in the next step whether PAFB enters the cells actively or passively, e.g. by diffusion. To this end, we exposed 4.5 h-old germinated conidia to NaN_3 and carbonyl cyanide *m*-chlorophenylhydrazone (CCCP), which are inhibitors of oxidative phosphorylation and ATP production, respectively, for 30 min before BODIPY-PAFB was added for further 1.5 h of incubation.

As shown in Fig. 8, BODIPY-PAFB remained attached to the outer layers and was not taken up into the *N. crassa* cells in the presence of the inhibitors (Fig. 8). In contrast, BODIPY-PAFB localized in the vacuoles of germlings that were not exposed to the inhibitors (Fig. 8). PAFB uptake was also inhibited at 4 $^\circ\text{C}$, which reduces cell metabolism (data not shown).

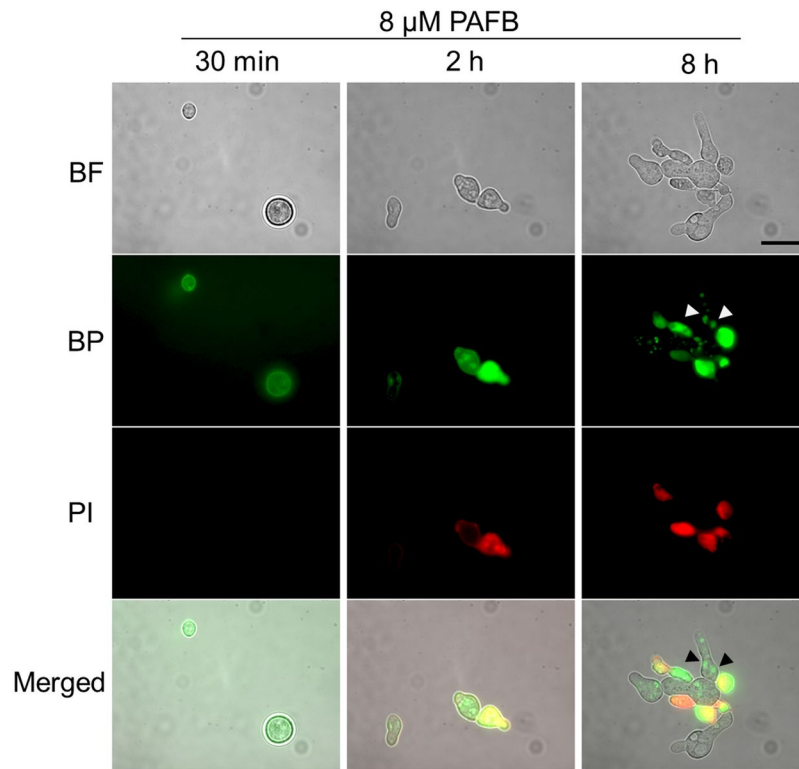


Figure 7. Uptake of BODIPY-PAFB (8 μ M) in *N. crassa* conidia or germlings. Samples were taken after 30 min, 2 h and 8 h and co-stained with PI for 10 min before imaging. White and black arrows indicate BP-PAFB specific signals in vacuoles. BF = Brightfield, BP = BODIPY-labelled PAFB. Scale bar = 15 μ m.

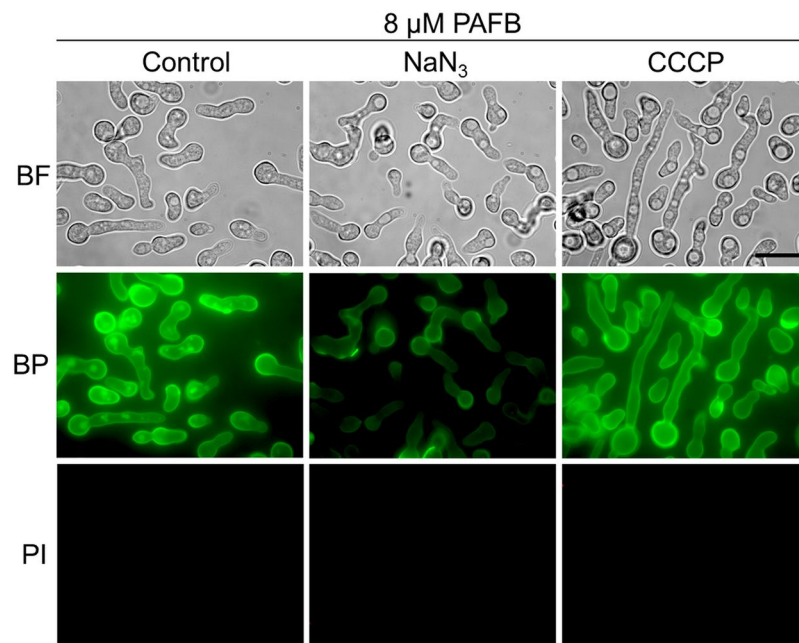


Figure 8. Uptake of BODIPY-PAFB (8 μ M) in *N. crassa* germlings in the presence of 100 μ M CCCP or 2.5 mM NaN_3 . The control was stained with BODIPY-PAFB without inhibitors. All samples were co-stained with PI for 10 min before imaging. BF = Brightfield, BP = BODIPY-labelled PAFB. Scale bar = 15 μ m.

These observations proved the staining specificity of BODIPY-PAFB and indicate that the internalization of BODIPY-PAFB depends on an active cellular metabolism. Negative PI staining confirmed the viability of the cells under the applied test conditions.

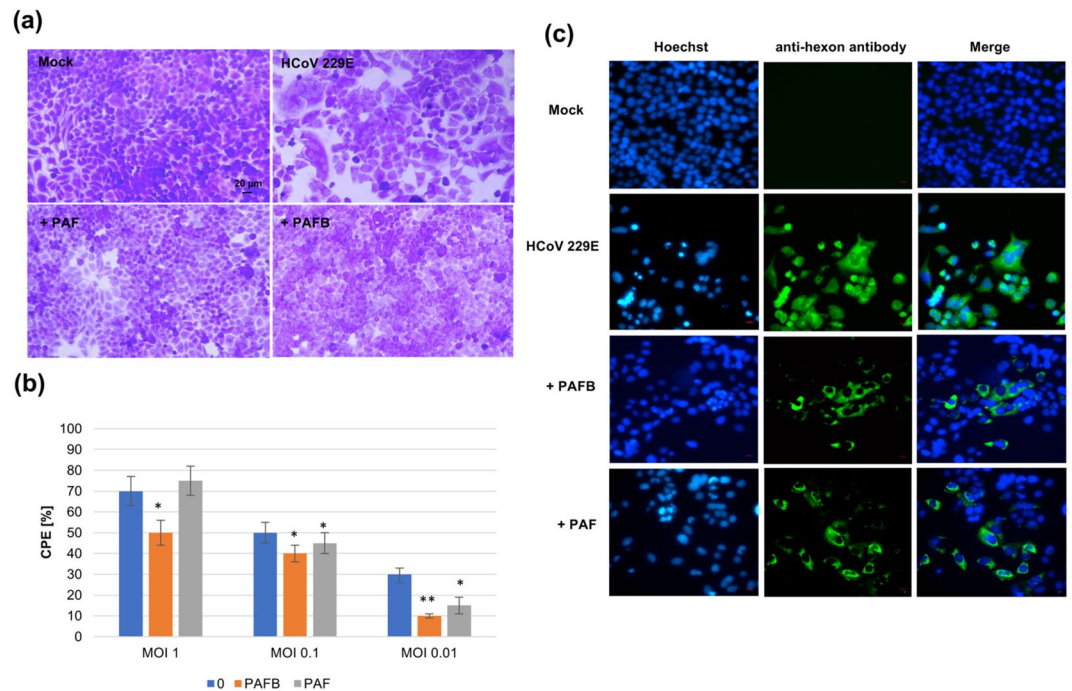


Figure 9. PAFB and PAF reduced CPE of HCoV 229E in L132 cells. PAFB and PAF (8 μM, respectively) were applied. **(a)** Crystal violet assay visualized the reduction of virus-induced CPE at MOI 0.01. **(b)** Reduction of the viral CPE at MOI 1, MOI 0.1 and MOI 0.01 at 72 h post infection in the presence of PAFB and PAF (0, untreated control). **(c)** Immunostaining of HCoV 229E protein in L132 cells with mouse-anti hexon antibody and goat anti-mouse FITC-labelled secondary antibody after treatment with PAFB and PAF. Nuclei of fixed L132 cells were counter-stained with Hoechst 33342. Virus-uninfected cells (Mock) served as a negative control and virus infected cells without protein treatment as positive control (HCoV 229E); * $p < 0.05$; ** $p < 0.01$.

Antiviral activity. Recently, Holthausen *et al.* (2017) reported about the efficacy of host defense peptides from the skin of the South Indian frog to treat respiratory viral infections, as in the case of human influenza A viruses²⁸. In this study, we examined the selective anti-viral potential of PAFB and PAF to reduce the infection of human epithelial cell line L132 by the human coronavirus strain 229E (HCoV 229E) *in vitro*. First, we confirmed that PAFB, similarly to PAF, showed no cytotoxic effects on the host cells in the applied concentration range (0–32 μM) (Supplementary Fig. S7). The anti-viral activity of the proteins was expressed in terms of protein concentration that protects against virus-induced cytopathogenic effects (CPE) in L132 cells, such as syncytia formation, vacuolization, cell rounding, detachment and cell death (Fig. 9a). We determined 8 μM as the minimum effective protein concentration that reduced virus-induced CPE and preserved cell monolayer integrity (Fig. 9a,b). The anti-viral efficiency could be observed in virus infected L132 cells at different viral titres (multiplicity of infection (MOI) 1–0.01) (Supplementary Fig. S8), but reached a maximum inhibition value of 21.07% with PAFB against HCoV 229E at MOI 0.01 (Fig. 9b). PAF in contrast, inhibited HCoV 229E-induced CPE less effectively than PAFB, while still exhibiting antiviral activity, especially at lower viral titres: 8 μM PAF reduced the viral CPE to 11.89% at MOI 0.01 (Fig. 9a,b). The application of higher protein concentrations (16 μM and 32 μM), however, did not further increase the anti-viral effect of PAFB and PAF (Supplementary Fig. S8). The anti-viral efficacy of both proteins was also confirmed by immunofluorescence experiments, where 8 μM PAFB and PAF successfully reduced the number of HCoV 229E infected L132 cells (Fig. 9c). HCoV 229E localization was examined with a virus-specific antibody at 72 h post infection when viral replication and transcription was underway. As shown in Fig. 9c, a strong virus-specific green fluorescent signal was observed in the majority of HCoV 229E infected cells (MOI 0.01) without PAFB or PAF treatment. The signal intensity and the number of virus infected cells significantly decreased in the presence of PAFB or PAF (Fig. 9c). This observation suggests that the antiviral effect of the proteins may reduce not only the final stages of the viral replication cycle and CPE, but also the earlier steps of the infection and/or the spread of the viral particles.

Discussion

In this study, we provide detailed insight into the antimicrobial activity and the structure of the secreted PAFB protein from the penicillin-producing mould *P. chrysogenum* Q176. This protein belongs to the group of small, cysteine-rich and cationic proteins from ascomycetes. Although the PAFB encoding gene was abundantly transcribed, we could not detect the translated gene product under the cultivation conditions applied. This phenomenon is not unique. Only recently, Garrigues *et al.* (2016) reported that the identification of the genome encoded antifungal protein AfpB from *Penicillium digitatum* had failed, although the gene was transcribed at high level¹⁸. Instead the antifungal activity of this cryptic protein was successfully analysed by mapping the antifungal motifs of AfpB with synthetic cysteine-containing peptides²⁹ before recombinant, full-length AfpB was generated

recently for functional analysis applying the *P. chrysogenum*-based expression system^{20,30}. The reason remains obscure, why the timely expressed and correctly processed *pafB* mRNA was not translated into detectable protein amounts by *P. chrysogenum* Q176. As conidia of *P. chrysogenum* were PAFB susceptible, it seems that the production of PAFB needs strict regulation to avoid self-limitation. On the other hand, the pre-existing pool of mRNA may serve as a reservoir allowing for fast availability in case of urgent needs, e.g. a fast response to changing environmental or developmental stimuli. Indeed, a function of cysteine-rich, cationic proteins beyond fungal growth inhibition, such as stress response and asexual development, supporting the fitness of the producing moulds has been reported earlier^{21,31}. A recently published transcriptome meta-analysis for the expression regulation of the *Aspergillus niger* antifungal protein AnAFP further underlines the role of these proteins in stress response, growth and development, nutrient recycling, and autophagy³². Thus, the *pafB* mRNA may be stored, for example in processing bodies or stress granules as described for *S. cerevisiae* and mammalian cells, until the PAFB protein is needed^{33–35}. We are currently investigating this assumption.

We applied the *P. chrysogenum*-based expression system to generate PAFB in sufficient quantity and high quality for functional and structural analyses. The strong *paf* promoter, the presence of multiple gene copies and/or possibly the genomic integration site are responsible for the bulk production of recombinant PAFB^{20,36}. The fact that recombinant PAFB was produced in *P. chrysogenum* Δpaf without problems indicates that regulatory elements, likely present in the 5'- and/or 3'- regions of the *pafB* mRNA and responsible for controlling mRNA translation and/or storage in the wild-type, were replaced in the *pafB* expression cassette.

Mature PAFB was purified in a major full-length form with 58 aa, and two less abundant short variants with 57 aa and 56 aa, respectively. Another member of this protein group, the *Aspergillus giganteus* AFP, is secreted in two naturally occurring N-terminal variants, the major short form (51 aa) and in lower amounts the larger form (Lf-AFP), containing six additional N-terminal amino acids³⁷. Lf-AFP remarkably differs from AFP in pI, GRAVY and net charge and shows lower antifungal activity^{37,38}. To date, we cannot tell whether the N-terminal PAFB variants occur naturally, e.g. by autocatalytic activities, or whether they are a consequence of overexpression conditions. The latter has been observed for example, for the expression of the recombinant bovine chymosin in *Aspergillus awamori*, which resulted in products with variable N-termini, most likely due to proteolysis in the culture supernatant³⁹. Recombinant PAF produced in high yields in *P. chrysogenum* showed no N-terminal variations whereas subtle N-terminal differences were detected when expressed in *P. digitatum*²⁰. Similarly, AfpB expression in *P. digitatum* using the *paf*-derived expression cassette resulted in gene products with N-terminal variations³⁰. In none of these cases, however, the antifungal activity of the N-terminal variants was affected^{20,30}. Proteolysis of the PAFB N-terminus might be influenced by the nutrient composition of the fermentation broth. For double isotope labelling (¹⁵N/¹³C) of PAFB, sucrose was replaced with ¹³C-glucose as carbon source in the growth medium, which might be responsible for the generation of sfPAFB (56 aa). This assumption requires further analysis in the future. In one of our recent studies, we demonstrated that the N-terminal aa regulate the stability, folding and antifungal function of the recombinant NFAP protein from *Neosartorya fischeri*⁴⁰. By contrast, we found here, that the N-terminal PAFB variants do not differ significantly in their overall solution structure and physico-chemical features. We therefore assume that the antifungal activity is not affected.

Importantly, the mature full-length PAFB is identical to the mature PgAFP described from *P. chrysogenum* RP42C, originally isolated from cured ham⁴¹. PgAFP was shown to be sensitive to the ionic strength of the fungal culture medium⁴², and highly stable under extreme pH, high temperature and against proteolysis¹⁹. This is also true for other members of this antifungal protein group, such as PAF, AFP, or NFAP, which possess a highly stable disulphide-bond mediated, compact, β -fold structure^{9,40,43}.

PAFB showed potent antifungal activity against model fungi and human fungal pathogens in low concentrations (μ M range). PAFB prevented more effectively than PAF the germination and colony establishment of *N. crassa*, and significant differences in the susceptibility of some tested fungi, e.g. *A. terreus*, *P. chrysogenum*, point towards different modes of action of these two proteins. Variations in the antifungal spectrum and the mode of action were reported for the structurally very similar, related antifungal proteins PAF, AfpB, NFAP and AFP^{26,30,44,45}. We propose that the presence and activity of host interaction molecules that regulate the uptake mechanism, the processing of signals and the ability to cope with detrimental effects triggered by the antifungal proteins determine the susceptibility of fungal species. Furthermore, the importance of protein surface charges and their distributions described for PAF function need to be considered to explain differences in the antifungal activity⁸.

Recombinant PAFB was identified after 72 h of cultivation and reached its maximum amount after 96 h in the standard medium MM, which perfectly coincided with the onset of production of PAF and other recombinant PAF variants that had been generated with this expression system under the control of the *paf* promoter²⁰. Interestingly, the overproduction of recombinant PAFB did not affect the proliferation of the producer strain *P. chrysogenum pafB*, although an inhibitory activity was observed on conidia in the microdilution assays (Table 1). One possible explanation for this phenomenon could be that under PAFB expression conditions (established hyphal growth and MM), *P. chrysogenum* hyphae lack any PAFB susceptibility determinants, which, in contrast, must be present in $0.1 \times$ PDB. Indeed, we proved that PAFB, similarly to PAF, did not interact with *P. chrysogenum* hyphae cultivated in MM (Supplementary Fig. S9). Only when grown in $0.1 \times$ PDB, hyphal proliferation was inhibited and PAFB was taken up by the cells (Supplementary Fig. S9). PAF, on the other hand, neither interacted with *P. chrysogenum* conidia nor hyphae, irrespective of the culture medium applied (Table 1 and Supplementary Fig. S9).

Similar nutrient dependent susceptibility for PAFB and PAF was observed with yeasts. Up to date, potent anti-yeast activity was only reported for the *N. fischeri* protein NFAP2, which killed yeast cells within minutes by plasma membrane disruption¹. Neither for PgAFP¹⁹, nor for the related proteins AFP, NFAP and PAF any yeast inhibitory activity was ever found^{1,46}. Most interestingly, in this study we show for the first time, anti-yeast activity of PAFB and PAF in $10 \times$ diluted PDB. Apparently, yeast cells exhibit susceptibility determinants for both proteins

when cultivated in this “starvation” medium. The time course experiments indicated that *C. albicans* cells were not killed immediately after administration of PAFB and PAF, but that cell death occurred in a time and concentration dependent manner, supporting our observations made so far that exclude a fast killing mechanism, e.g. by pore formation, but point towards more complex interaction mechanisms with the target cell^{8,27}.

Indeed, cell toxicity of PAFB in all susceptible fungi studied correlated with active protein internalization and its subsequent distribution in the cytoplasm, which coincided with PI positive staining as observed with PAF and other antifungal peptides and proteins in previous studies^{8,22,47–49}. Higher fungicidal activity of PAFB over that of PAF might result from differences in efficient uptake and/or reaching an effective killing concentration within the cell. Further investigations are needed to elucidate the mechanisms that regulate fungal susceptibility and killing kinetics of members of this protein group.

Few studies were published on the anti-viral activity of antimicrobial peptides and proteins expressed by animals and plants, e.g. defensins^{50–52}. A surprising and novel observation for small, cysteine-rich, cationic and antimicrobial proteins of fungal origin was the efficacy of PAFB and PAF against HCoV 229E virus. This virus is highly contagious and can cause mild, cold-like respiratory illness. However, highly pathogenic HCoVs such as severe acute respiratory syndrome CoV (SARS-CoV) and Middle East respiratory syndrome CoV (MERS-CoV) predominantly infect lower airways and cause fatal pneumonia with high morbidity and mortality during an epidemic⁵³. Anti-HCoV drugs and vaccines are in different stages of development, but they are still lacking today⁵⁴. PAFB and PAF, preferentially at low MOI, reduced the virus-induced CPE of infected human L132 cells, thus promising a potential alternative therapeutic approach against human coronaviruses. Based on the data collected in this study, we suggest that PAFB and PAF directly - or indirectly by influencing the host cell metabolism - inhibit the release and spread of progeny virus particles, or destroy the HCoV virions. The observed slight differences in the anti-viral activity between PAFB and PAF may result from different virus or host cell susceptibility towards both proteins, or from differences in the protein surface charge distributions as outlined above. The observation that anti-viral efficacy could not be further increased with higher protein concentrations than 8 µM could be attributed to low bioavailability of the proteins at higher concentrations, a partial clustering or hampered crossing of bio-membranes as shown for antimicrobial proteins in previous studies^{55,56}. Work is currently in progress to get detailed insight into the mode of the anti-viral action of PAFB and PAF.

Importantly, lethal activity of the potential drugs towards human cells has to be excluded and harmful side effects need to be kept to a minimum for future antimicrobial drug development. Similar to AFP and PAF^{10,57}, no toxic activity on mammalian cells was detected for PAFB *in vitro* (Supplementary Fig. S7). This feature and the antifungal/antiviral potential render PAFB a promising candidate for the development of novel antimicrobial treatment strategies.

Methods

Strains, media and cultivation conditions. Microbial strains used in this study and growth media are listed in the Supplementary Table S2 and Table S3, respectively.

The propagation of vectors and plasmids was carried out in *E. coli* DH5α, grown in lysogeny broth medium (LB), supplemented with 100 µg/mL ampicillin. Yeasts were grown on potato dextrose agar (PDA, Becton Dickinson) or on solid yeast extract peptone dextrose medium (YPD) at 37 °C.

For the generation of conidia, *P. chrysogenum* was cultivated on solid defined minimal medium (MM) at 25 °C, *N. crassa* on Vogel's agar plates at 37 °C under continuous light and *A. fumigatus*, *A. niger* and *A. terreus* were grown on PDA (Becton Dickinson) at 37 °C. *T. rubrum* was grown on oatmeal agar. Conidia were harvested in spore buffer (0.9% NaCl (w/v), 0.01% Tween 80 (v/v)). For transformation, 10⁸ conidia of *P. chrysogenum* Δ*paf*²¹ were grown in 200 mL CM for 38 h at 25 °C under continuous shaking (210 rpm). Conidia (1–2 × 10⁸) of *P. chrysogenum* Q176 and *P. chrysogenum pafB* were cultivated in 200 mL MM for 24–144 h at 25 °C under continuous shaking for Northern, Southern and Western blot analyses and PAFB production, respectively. PAFB single (¹⁵N) or double (¹⁵N/¹³C) isotope-labelling for NMR analysis was carried out by replacing the nitrogen and/or carbon source in MM by 0.3% Na¹⁵NO₃ and/or 1% ¹³C-glucose (w/v) (Euriso-Top), respectively.

Northern analysis. Total RNA was isolated from *P. chrysogenum* Q176 liquid cultures using TRI Reagent (Sigma-Aldrich). Ten µg RNA per lane were loaded on 1.2% formaldehyde-agarose gels, blotted onto Hybond-N membranes (Amersham Biosciences) and hybridized with digoxigenin (DIG)-labelled probes (Roche). The primer pair *opafB_fw/opafB_rev* and *opaf1_fw/opaf1_rev* was used for PCR-based amplification of the *pafB* and *paf* specific hybridization probes, respectively (Supplementary Table S4).

Fungal transformation and verification of plasmid integration. For the generation of a PAFB-overproducing *P. chrysogenum* strain, the *paf* deletion mutant *P. chrysogenum* Δ*paf*²¹ was transformed with pSK275*pafB*. Protoplast formation and transformation of 10 µg *Pst*I linearized pSK275*pafB* was carried out according to Cantoral *et al.*⁵⁸. Transformants were single spored three times on MM agar supplemented with 0.3–0.6 µg/mL pyrithiamine hydrobromide (Sigma-Aldrich).

Positive transformants were analysed by Southern blotting for the genomic integration of pSK275*pafB*²⁰. A detailed description is given in the Supplementary Methods.

Protein expression, purification and verification. PAFB and PAF were produced and purified from the cell-free supernatant as recently described²⁰. To verify the identity of purified PAFB, the protein mass was determined by ESI-MS at the Protein Micro-Analysis Facility (Medical University of Innsbruck)²⁰. In addition, protein solution was size-fractionated on a 18% (w/v) SDS-PAGE as described²⁰.

NMR analyses. Three PAFB samples were prepared for NMR studies: an unlabelled, a ^{15}N -labelled and a $^{15}\text{N}/^{13}\text{C}$ -labelled as described recently²⁰. Lyophilized protein was dissolved in 20 mM acetate buffer (prepared with deuterated acetic acid, pH = 4.5) and filled into Shigemitsu NMR sample tube (250 μL). Protein concentration was set to 1.5 mM. Protein resonance assignment was accomplished with the same strategy that was applied previously for double-labelled PAF⁶. Briefly, 2D ^{15}N -HSQC served as the root for the following 3D triple resonance experiments: HNC(O), HN(CA)CO, HNCA, HN(CO)CA, HNCACB, HNHA, HBHA(CO)NH and HN(CO)CACB, which were used for obtaining backbone signal assignments⁵⁹. For resonance assignment of side chains the combination of HC(C)H COSY, HC(C)H TOCSY, HCC(CO)NH and (H)CCH-TOCSY experiments were used, and aromatic protons were identified with the aid of 2D CB(CGCD)HD and CB(CGCDCE)HE spectra. The applied experiment versions were identical with those described in our previous study⁶. To collect NOE distance restraints, ^{15}N - and ^{13}C -resolved 3D NOESY spectra were recorded as well as a 2D ^1H - ^1H NOESY this latter experiment was performed on the unlabelled PAFB sample. All the above listed measurements were recorded on a Bruker Avance II 500 spectrometer equipped with TXI z-gradient probe-head. The NOESY-type experiments were repeated on a 700 MHz spectrometer with similar configuration. The higher spectral resolution of the NOESY spectra with less overlapping cross-peaks help obtaining more distant restraints for structure calculation. All spectra were acquired at 298 K and data was processed with Topspin 3.0 software. Sequential resonance assignment was performed with the aid of CARA 1.8.4 software from which chemical shift data was exported to other software. Cyana 2.1 torsion angle dynamics package^{60,61} was used for *de novo* structure determination in combination with the ATNOS-CANDID algorithm (the latter was used for peak picking and NOE assignment). Setup files for Cyana were prepared manually. Disulphide connections were defined in the Cyana input assuming *abcabc* disulphide pattern as in PAF (linking cysteine 8–36, 15–43 and 28–54). Diastereotopic protons for non-equivalent CH_2 groups were considered as stereo-chemically ambiguous assignments. Backbone torsional angle constraints were predicted according to TALOS+⁶² and were used for the refinement of the structure model. Seven cycles of Cyana iterations were performed, and the 20 lowest energy conformers were considered as a final structure model. Chemical shift data and NMR experimental parameters were submitted to the BMRB databank and the structural ensemble was uploaded to Protein Data Bank (ID: 2NC2).

Antibacterial and antifungal activity assays. Growth inhibition assays were performed in 96-well microtiter plates (Nunclon Delta, Thermo Scientific). Conidia or yeast cells ($10^4/\text{mL}$) were incubated in $0.1 \times \text{PDB}$ (Becton Dickinson) with increasing concentrations of PAFB (0–32 μM) in a total volume of 200 μL at 25–30 °C. Bacteria were pre-cultivated in $0.1 \times \text{LB}$ or $0.1 \times \text{PDB}$ to reach OD_{620} of 0.05 and then exposed to antimicrobial treatment (0–32 μM PAFB) at 37 °C. Microbial growth was monitored after 24–48 h by measuring the OD_{620} with a Fluostar Omega microplate reader (BMG Labtech) and microscopically using an inverted microscope (Leica DM IL Led, Leica Microsystems). Images were taken with an AxioCam MR digital camera (Carl Zeiss GmbH) and processed with AxioVision software (Carl Zeiss GmbH). The MIC was defined as the minimal protein concentration that inhibited growth by $\geq 90\%$ compared to the untreated control which was referred as 100% growth.

The germination efficiency and germ tube length of *N. crassa* in the presence of PAFB at its MIC was determined as described⁸.

Fungistatic and fungicidal effects on *C. albicans* were determined by incubating 2×10^4 cells per mL in $0.1 \times \text{PDB}$ with 0–4 μM PAFB at 30 °C with shaking for up to 24 h. Samples were taken after 0 h, 6 h and 24 h, diluted in $0.1 \times \text{PDB}$ and plated on PDA plates in duplicates. The number of colony forming units was determined after incubating the plates for 24–48 h at 37 °C. The survival rate was calculated by setting the colony forming units at time point 0 h as 100%.

In all experiments 0–32 μM PAFB was applied for comparison. Experiments were prepared in technical triplicates and performed at least twice.

Uptake and localization studies. The green fluorophore BODIPY FL EDA (Life Technologies) was used for protein labelling as described by Sonderegger *et al.*⁸.

To study the protein uptake into *C. albicans*, *P. chrysogenum* and *N. crassa*, 10^6 yeast cells/mL or conidia/mL were incubated with 8 μM BODIPY-labelled proteins in the respective media ($0.1 \times \text{PDB}$, $0.2 \times \text{Vogel's}$) at 25–30 °C and analysed within an incubation time of 30 min to 12 h. To investigate PAFB uptake into *P. chrysogenum* hyphae grown in MM, 24 h old mycelia were stained with 8 μM BODIPY-labelled PAFB for 2.5 h.

Co-staining with 5 $\mu\text{g}/\text{mL}$ PI for 10 min at room temperature was carried out to monitor the viability of fungal cells. For positive staining controls, samples were treated with 50% (v/v) ethanol for 30 min.

PAFB-transport into hyphae was investigated in *N. crassa*. Conidia ($5 \times 10^5/\text{mL}$) were grown in $0.2 \times \text{Vogel's}$ medium for 4.5 h at 25 °C and then further incubated at 4 °C or with 2.5 mM NaN_3 (Sigma-Aldrich) or 100 μM CCCP (Sigma-Aldrich) for 30 min, respectively. BODIPY-labelled PAFB (8 μM) was added and the samples were microscopically analysed after 1.5 h of incubation.

Microscopic imaging was performed with a fluorescence microscope (Axioplan, Carl Zeiss GmbH), equipped with an AxioCam MR3 camera (excitation/emission filters 500/535 nm for green fluorescence, 546/590 or 565/620 nm for red fluorescence, Carl Zeiss GmbH). Image processing and editing was done with Axiovision (Carl Zeiss GmbH), GIMP (GNU Image Manipulation Program, version 2.8.20; www.gimp.org) and Microsoft Power Point (Microsoft Corp.).

Antiviral activity assays

Cultivation of human epithelial cell line L132. For virus propagation L132 cells were grown in antibiotic-free Dulbecco's Modified Eagle Medium with nonessential amino acids (Thermo Fisher Scientific) complemented with 10% fetal bovine serum (FBS, Eurobio). For the antiviral assays the same medium was used, containing only 2% FBS.

Viruses. The human coronavirus HCoV 229E was propagated and quantified in L132 cells. Initial virus titers were calculated as 50% cell culture infectious doses (CCID₅₀/mL), according to Reed and Muench (1938)⁶³. All virus stocks were stored at -70°C until used.

Antiviral tests. The antiviral activity of PAFB and PAF was determined by evaluating the reduction of the virus-induced CPE, characterized by rounding, vacuolization, syncytia formation and cell death of the cell monolayer. One day before infection, 1×10^4 L132 cells/well were seeded into a 96-well culture plate. The next day, medium was replaced by fresh medium containing diluted virus suspension at MOI 0.01–1.0 was added to the cell culture, followed by the immediate addition of cell culture medium supplemented with 2% FBS and 0–32 μM PAFB or PAF. Plates were then incubated at 33°C , 5% CO_2 , for HCoV 229E strain, and checked for virus-induced CPE after 24 h and 72 h, using an inverted light microscope AE2000 (Motic).

The antiviral activity of the proteins was determined by the crystal violet assay, adapted from Feoktistova *et al.*⁶⁴. Antiviral activity was expressed as the percentage effective CPE-inhibitory concentration. Modification of the cell morphology and reduction of the virus-induced CPE were also microscopically determined. Three independent experiments were carried out in triplicate.

For immunofluorescence staining, L132 cells were fixed in 3.7% (v/v) formaldehyde (Sigma-Aldrich) and subsequently immersed in PBS containing 0.1% (v/v) Triton X-100 for cell permeabilization. Samples were blocked in PBS/3% BSA (w/v) (Sigma-Aldrich). Hoechst 33342 (Thermo Fischer Scientific) was used as nuclear counterstains for fixed cells. The viral capsid was detected by mouse monoclonal anti-hexon antibody (1:100) (Santa Cruz Biotechnology) diluted in PBS/3% (w/v) BSA. Primary antibodies were incubated on the fixed cells for 90 min at room temperature, washed, and the antigen-antibody complexes were detected with goat anti-mouse FITC-labelled secondary antibody (1:1,000) (Santa Cruz Biotechnology) according to Grigorov *et al.*⁶⁵. Images were acquired using an inverted epifluorescence microscope (Axio Observer 3, Carl Zeiss GmbH). Imaging and image processing was routinely performed with ZEN software (2009, Carl Zeiss GmbH) or ImageJ (The ImageJ ecosystem: An open platform for biomedical image analysis)⁶⁶.

Statistical analyses. Statistical analysis was performed using Microsoft Excel 2010 software (Microsoft Corp.). Two sample t-test with equal variance and one-tailed distribution was used.

Data availability. All data generated or analysed during this study are included in this published article (and its Supplementary Information files).

References

- Toth, L. *et al.* NFAP2, a novel cysteine-rich anti-yeast protein from *Neosartorya fischeri* NRRL 181: isolation and characterization. *AMB Express* **6**, 75, <https://doi.org/10.1186/s13568-016-0250-8> (2016).
- Jami, M. S., Barreiro, C., García-Estrada, C. & Martín, J. F. Proteome analysis of the penicillin producer *Penicillium chrysogenum*: characterization of protein changes during the industrial strain improvement. *Mol Cell Proteomics* **9**, 1182–1198, <https://doi.org/10.1074/mcp.M900327-MCP200> (2010).
- Hoff, B., Pöggeler, S. & Kück, U. Eighty years after its discovery, Fleming's *Penicillium* strain discloses the secret of its sex. *Eukaryot Cell* **7**, 465–470, <https://doi.org/10.1128/EC.00430-07> (2008).
- van den Berg, M. A. *et al.* Genome sequencing and analysis of the filamentous fungus *Penicillium chrysogenum*. *Nat Biotechnol* **26**, 1161–1168, <https://doi.org/10.1038/nbt.1498> (2008).
- Specht, T., Dahlmann, T. A., Zadra, I., Kürsteiner, H. & Kück, U. Complete Sequencing and chromosome-scale genome assembly of the industrial progenitor strain P2niaD18 from the penicillin producer *Penicillium chrysogenum*. *Genome Announc* **2**, <https://doi.org/10.1128/genomeA.00577-14> (2014).
- Fizil, Á., Gáspári, Z., Barna, T., Marx, F. & Batta, G. “Invisible” conformers of an antifungal disulfide protein revealed by constrained cold and heat unfolding, CEST-NMR experiments, and molecular dynamics calculations. *Chemistry* **21**, 5136–5144, <https://doi.org/10.1002/chem.201404879> (2015).
- Marx, F., Binder, U., Leiter, É. & Pócsi, I. The *Penicillium chrysogenum* antifungal protein PAF, a promising tool for the development of new antifungal therapies and fungal cell biology studies. *Cell Mol Life Sci* **65**, 445–454, <https://doi.org/10.1007/s00018-007-7364-8> (2008).
- Sonderegger, C. *et al.* D19S mutation of the cationic, cysteine-rich protein PAF: novel insights into its structural dynamics, thermal unfolding and antifungal function. *PLoS One* **12**, <https://doi.org/10.1371/journal.pone.0169920> (2017).
- Batta, G. *et al.* Functional aspects of the solution structure and dynamics of PAF, a highly stable antifungal protein from *Penicillium chrysogenum*. *FEBS J* **276**, 2875–2890, <https://doi.org/10.1111/j.1742-4658.2009.07011.x> (2009).
- Szappanos, H. *et al.* The *Penicillium chrysogenum*-derived antifungal peptide shows no toxic effects on mammalian cells in the intended therapeutic concentration. *Naunyn Schmiedebergs Arch Pharmacol* **371**, 122–132, <https://doi.org/10.1007/s00210-004-1013-7> (2005).
- Palicz, Z. *et al.* *In vivo* application of a small molecular weight antifungal protein of *Penicillium chrysogenum* (PAF). *Toxicol Appl Pharmacol* **269**, 8–16, <https://doi.org/10.1016/j.taap.2013.02.014> (2013).
- Palicz, Z. *et al.* Application of a low molecular weight antifungal protein from *Penicillium chrysogenum* (PAF) to treat pulmonary aspergillosis in mice. *Emerg Microbes Infect* **5**, <https://doi.org/10.1038/emi.2016.116> (2016).
- Barna, B., Leiter, É., Hegeudés, N., Bíró, T. & Pócsi, I. Effect of the *Penicillium chrysogenum* antifungal protein (PAF) on barley powdery mildew and wheat leaf rust pathogens. *J Basic Microbiol* **48**, 516–520, <https://doi.org/10.1002/jobm.200800197> (2008).
- Marx, F. *et al.* Cloning, structural organization and regulation of expression of the *Penicillium chrysogenum* *paf* gene encoding an abundantly secreted protein with antifungal activity. *Gene* **167**, 167–171 (1995).
- Chen, Z. *et al.* Purification and characterization of a novel antifungal protein secreted by *Penicillium chrysogenum* from an arctic sediment. *Appl Microbiol Biotechnol* **97**, 10381–10390, <https://doi.org/10.1007/s00253-013-4800-6> (2013).
- Seibold, M., Wolschann, P., Bodevin, S. & Olsen, O. Properties of the bubble protein, a defensin and an abundant component of a fungal exudate. *Peptides* **32**, 1989–1995, <https://doi.org/10.1016/j.peptides.2011.08.022> (2011).
- Rodríguez-Martín, A. *et al.* Characterization of the novel antifungal protein PgAFP and the encoding gene of *Penicillium chrysogenum*. *Peptides* **31**, 541–547, <https://doi.org/10.1016/j.peptides.2009.11.002> (2010).
- Garrigues, S., Gandia, M. & Marcos, J. F. Occurrence and function of fungal antifungal proteins: a case study of the citrus postharvest pathogen *Penicillium digitatum*. *Appl Microbiol Biotechnol* **100**, 2243–2256, <https://doi.org/10.1007/s00253-015-7110-3> (2016).
- Delgado, J. *et al.* Growth inhibition and stability of PgAFP from *Penicillium chrysogenum* against fungi common on dry-ripened meat products. *Int J Food Microbiol* **205**, 23–29, <https://doi.org/10.1016/j.ijfoodmicro.2015.03.029> (2015).

20. Sonderegger, C. *et al.* A *Penicillium chrysogenum*-based expression system for the production of small, cysteine-rich antifungal proteins for structural and functional analyses. *Microb Cell Fact* **15**, 192, <https://doi.org/10.1186/s12934-016-0586-4> (2016).
21. Hegedűs, N., Sigl, C., Zadra, I., Pócsi, I. & Marx, F. The *pag* gene product modulates asexual development in *Penicillium chrysogenum*. *J Basic Microbiol* **51**, 253–262, <https://doi.org/10.1002/jobm.201000321> (2011).
22. Oberparleiter, C. *et al.* Active internalization of the *Penicillium chrysogenum* antifungal protein PAF in sensitive aspergilli. *Antimicrob Agents Chemother* **47**, 3598–3601, <https://doi.org/10.1128/AAC.47.11.3598-3601.2003> (2003).
23. Tazi, J., Bakkour, N. & Stamm, S. Alternative splicing and disease. *Biochim Biophys Acta* **1792**, 14–26, <https://doi.org/10.1016/j.bbadis.2008.09.017> (2009).
24. Wessagowit, V., Nalla, V. K., Rogan, P. K. & McGrath, J. A. Normal and abnormal mechanisms of gene splicing and relevance to inherited skin diseases. *J Dermatol Sci* **40**, 73–84, <https://doi.org/10.1016/j.jdermsci.2005.05.006> (2005).
25. Gasteiger, E. *et al.* Protein identification and analysis tools on the ExPASy server in *The proteomics protocols handbook* (ed. Walker, J. M.) 571–607 (Humana Press 2005).
26. Kaiserer, L. *et al.* Characterization of the *Penicillium chrysogenum* antifungal protein PAF. *Arch Microbiol* **180**, 204–210, <https://doi.org/10.1007/s00203-003-0578-8> (2003).
27. Binder, U., Chu, M., Read, N. D. & Marx, F. The antifungal activity of the *Penicillium chrysogenum* protein PAF disrupts calcium homeostasis in *Neurospora crassa*. *Eukaryot Cell* **9**, 1374–1382, <https://doi.org/10.1128/EC.00050-10> (2010).
28. Holthausen, D. J. *et al.* An amphibian host defense peptide is virucidal for human H1 hemagglutinin-bearing influenza viruses. *Immunity* **46**, 587–595, <https://doi.org/10.1016/j.immuni.2017.03.018> (2017).
29. Garrigues, S. *et al.* Mapping and identification of antifungal peptides in the putative antifungal protein AfpB from the filamentous fungus *Penicillium digitatum*. *Front Microbiol* **8**, 592, <https://doi.org/10.3389/fmicb.2017.00592> (2017).
30. Garrigues, S. *et al.* Efficient production and characterization of the novel and highly active antifungal protein AfpB from *Penicillium digitatum*. *Sci Rep* **7**, <https://doi.org/10.1038/s41598-017-15277-w> (2017).
31. Eigentler, A., Pócsi, I. & Marx, F. The *anisin1* gene encodes a defensin-like protein and supports the fitness of *Aspergillus nidulans*. *Arch Microbiol* **194**, 427–437, <https://doi.org/10.1007/s00203-011-0773-y> (2012).
32. Paegle, N. *et al.* A transcriptome meta-analysis proposes novel biological roles for the antifungal protein AnAFP in *Aspergillus niger*. *PLoS One* **11**, <https://doi.org/10.1371/journal.pone.0165755> (2016).
33. Aizer, A. *et al.* Quantifying mRNA targeting to P-bodies in living human cells reveals their dual role in mRNA decay and storage. *J Cell Sci* **127**, 4443–4456, <https://doi.org/10.1242/jcs.152975> (2014).
34. Gray, N. K., Hrabáková, L., Scanlon, J. P. & Smith, R. W. Poly(A)-binding proteins and mRNA localization: who rules the roost? *Biochem Soc Trans* **43**, 1277–1284, <https://doi.org/10.1042/BST20150171> (2015).
35. Pizzinga, M. & Ashe, M. P. Yeast mRNA localization: protein asymmetry, organelle localization and response to stress. *Biochem Soc Trans* **42**, 1256–1260, <https://doi.org/10.1042/Bst20140086> (2014).
36. Gerasimova, T. I. & Corces, V. G. Chromatin insulators and boundaries: effects on transcription and nuclear organization. *Annu Rev Genet* **35**, 193–208, <https://doi.org/10.1146/annurev.genet.35.102401.090349> (2001).
37. Martínez-Ruiz, A. *et al.* Characterization of a natural larger form of the antifungal protein (AFP) from *Aspergillus giganteus*. *Biochim Biophys Acta* **1340**, 81–87, [https://doi.org/10.1016/S0167-4838\(97\)00038-1](https://doi.org/10.1016/S0167-4838(97)00038-1) (1997).
38. López-García, B. *et al.* Production of the biotechnologically relevant AFP from *Aspergillus giganteus* in the yeast *Pichia pastoris*. *Protein Expr Purif* **70**, 206–210, <https://doi.org/10.1016/j.pep.2009.11.002> (2010).
39. Cardoza, R. E. *et al.* Expression of a synthetic copy of the bovine *chymosin* gene in *Aspergillus awamori* from constitutive and pH-regulated promoters and secretion using two different pre-pro sequences. *Biotechnol Bioeng* **83**, 249–259, <https://doi.org/10.1002/bit.10666> (2003).
40. Galgóczy, L. *et al.* Structural determinants of *Neosartorya fischeri* antifungal protein (NFAP) for folding, stability and antifungal activity. *Sci Rep* **7**, 1963, <https://doi.org/10.1038/s41598-017-02234-w> (2017).
41. Acosta, R., Rodríguez-Martín, A., Martín, A., Núñez, F. & Asensio, M. A. Selection of antifungal protein-producing molds from dry-cured meat products. *Int J Food Microbiol* **135**, 39–46, <https://doi.org/10.1016/j.ijfoodmicro.2009.07.020> (2009).
42. Delgado, J., Owens, R. A., Doyle, S., Núñez, F. & Asensio, M. A. Quantitative proteomics reveals new insights into calcium-mediated resistance mechanisms in *Aspergillus flavus* against the antifungal protein PgAFP in cheese. *Food Microbiol* **66**, 1–10, <https://doi.org/10.1016/j.fm.2017.03.015> (2017).
43. Campos-Olivas, R. *et al.* NMR solution structure of the antifungal protein from *Aspergillus giganteus*: evidence for cysteine pairing isomerism. *Biochemistry* **34**, 3009–3021, <https://doi.org/10.1021/bi00009a032> (1995).
44. Virágh, M. *et al.* Production of a defensin-like antifungal protein NFAP from *Neosartorya fischeri* in *Pichia pastoris* and its antifungal activity against filamentous fungal isolates from human infections. *Protein Expr Purif* **94**, 79–84, <https://doi.org/10.1016/j.pep.2013.11.003> (2014).
45. Meyer, V. A small protein that fights fungi: AFP as a new promising antifungal agent of biotechnological value. *Appl Microbiol Biotechnol* **78**, 17–28, <https://doi.org/10.1007/s00253-007-1291-3> (2008).
46. Marx, F. Small, basic antifungal proteins secreted from filamentous ascomycetes: a comparative study regarding expression, structure, function and potential application. *Appl Microbiol Biotechnol* **65**, 133–142, <https://doi.org/10.1007/s00253-004-1600-z> (2004).
47. Delgado, J., Owens, R. A., Doyle, S., Asensio, M. A. & Núñez, F. Increased chitin biosynthesis contributes to the resistance of *Penicillium polonicum* against the antifungal protein PgAFP. *Appl Microbiol Biotechnol* **100**, 371–383, <https://doi.org/10.1007/s00253-015-7020-4> (2016).
48. El-Mounadi, K., Islam, K. T., Hernández-Ortiz, P., Read, N. D. & Shah, D. M. Antifungal mechanisms of a plant defensin MtDef4 are not conserved between the ascomycete fungi *Neurospora crassa* and *Fusarium graminearum*. *Mol Microbiol* **100**, 542–559, <https://doi.org/10.1111/mmi.13333> (2016).
49. Muñoz, A., López-García, B. & Marcos, J. F. Studies on the mode of action of the antifungal hexapeptide PAF26. *Antimicrob Agents Chemother* **50**, 3847–3855, <https://doi.org/10.1128/Aac.00650-06> (2006).
50. Lin, P., Wong, J. H. & Ng, T. B. A defensin with highly potent antipathogenic activities from the seeds of purple pole bean. *Biosci Rep* **30**, 101–109, <https://doi.org/10.1042/Bsr20090004> (2010).
51. Seidel, A. *et al.* Cyclic and acyclic defensins inhibit human immunodeficiency virus type-1 replication by different mechanisms. *PLoS One* **5**, e9737, <https://doi.org/10.1371/journal.pone.0009737> (2010).
52. Wang, G. Natural antimicrobial peptides as promising anti-HIV candidates. *Curr Top Pept Protein Res* **13**, 93–110 (2012).
53. Hui, D. S. Epidemic and Emerging coronaviruses (severe acute respiratory syndrome and middle east respiratory syndrome). *Clin Chest Med* **38**, 71–86, <https://doi.org/10.1016/j.ccm.2016.11.007> (2017).
54. Tang, J. W. *et al.* Global epidemiology of non-influenza RNA respiratory viruses: data gaps and a growing need for surveillance. *Lancet Infect Dis* **17**, 689, [https://doi.org/10.1016/S1473-3099\(17\)30238-4](https://doi.org/10.1016/S1473-3099(17)30238-4) (2017).
55. Fjell, C. D., Hiss, J. A., Hancock, R. E. & Schneider, G. Designing antimicrobial peptides: form follows function. *Nat Rev Drug Discov* **11**, 37–51, <https://doi.org/10.1038/nrd3591> (2011).
56. Mohanram, H. & Bhattacharjya, S. Resurrecting Inactive antimicrobial peptides from the lipopolysaccharide trap. *Antimicrob Agents Chemother* **58**, 1987–1996, <https://doi.org/10.1128/Aac.02321-13> (2014).
57. Szappanos, H. *et al.* The antifungal protein AFP secreted by *Aspergillus giganteus* does not cause detrimental effects on certain mammalian cells. *Peptides* **27**, 1717–1725, <https://doi.org/10.1016/j.peptides.2006.01.009> (2006).

58. Cantoral, J. M., Díez, B., Barredo, J. L., Alvarez, E. & Martín, J. F. High-frequency transformation of *Penicillium chrysogenum*. *Nat Biotechnol* **5**, 494–497 (1987).
59. Sattler, M., Schleucher, J. & Griesinger, C. Heteronuclear multidimensional NMR experiments for the structure determination of proteins in solution employing pulsed field gradients. *Prog Nucl Magn Reson Spectrosc* **34**, 93–158 (1999).
60. Herrmann, T., Güntert, P. & Wüthrich, K. Protein NMR structure determination with automated NOE assignment using the new software CANDID and the torsion angle dynamics algorithm DYANA. *J Mol Biol* **319**, 209–227, [https://doi.org/10.1016/S0022-2836\(02\)00241-3](https://doi.org/10.1016/S0022-2836(02)00241-3) (2002).
61. Herrmann, T., Güntert, P. & Wüthrich, K. Protein NMR structure determination with automated NOE-identification in the NOESY spectra using the new software ATNOS. *J Biomol NMR* **24**, 171–189, <https://doi.org/10.1023/A:1021614115432> (2002).
62. Shen, Y., Delaglio, F., Cornilescu, G. & Bax, A. TALOS+: a hybrid method for predicting protein backbone torsion angles from NMR chemical shifts. *J Biomol NMR* **44**, 213–223, <https://doi.org/10.1007/s10858-009-9333-z> (2009).
63. Reed, L. J. & Muench, H. A simple method of estimating fifty percent endpoints. *Am J Trop Med Hyg* **27**, 493–497 (1938).
64. Feoktistova, M., Geserick, P. & Leverkus, M. Crystal violet assay for determining viability of cultured cells. *Cold Spring Harb Protoc* **2016**, pdbprot087379, <https://doi.org/10.1101/pdb.prot087379> (2016).
65. Grigorov, B., Molle, J., Rubinstein, E., Zoulim, F. & Bartosch, B. CD81 large extracellular loop-containing fusion proteins with a dominant negative effect on HCV cell spread and replication. *J Gen Virol* **98**, 1646–1657, <https://doi.org/10.1099/jgv.0.000850> (2017).
66. Schindelin, J., Rueden, C. T., Hiner, M. C. & Eliceiri, K. W. The ImageJ ecosystem: An open platform for biomedical image analysis. *Mol Reprod Dev* **82**, 518–529, <https://doi.org/10.1002/mrd.22489> (2015).

Acknowledgements

We thank Julia Brindlinger and Evi Sirabella for technical assistance. This study was financially supported by the Austrian Science Fund FWF (I1644-B20 to FM), the Hungarian Science Fund OTKA (ANN 110821 to GB and NF 104198 to ZG) and the EU, co-financed by the European Regional Development Fund under the project GINOP-2.3.2-15-2016-00008. LG was financed with a Lise Meitner Fellowship from the FWF (M1776-B20) and a Postdoctoral Excellence Programme (PD 12808) from the Hungarian National Research, Development and Innovation (NKFI) Office. The research was further supported by the 700 MHz NMR spectrometer time provided by the MedInProt project of the Hungarian Academy of Sciences.

Author Contributions

F.M. and G.B. conceived, supervised and financed the study, designed experiments and edited the manuscript. A.H., D.B.-K. and L.G. analysed *pafB* and *paf* expression and PAFB and PAF production. A.H. and D.B.-K. produced recombinant PAFB and PAF. A.H., D.B.-K. and C.S. determined the antimicrobial activity. A.H. studied the protein uptake in fungi. M.V. and S.P. analysed the anti-viral potential. D.H., A.F., A.C., Z.G., Z.K., A.B. and G.B. investigated the structure of PAFB. All authors performed experiments, analysed and validated the data and helped to prepare the manuscript. All authors read, revised and approved the final manuscript version.

Additional Information

Supplementary information accompanies this paper at <https://doi.org/10.1038/s41598-018-20002-2>.

Competing Interests: The authors declare that they have no competing interests.

Publisher's note: Springer Nature remains neutral with regard to jurisdictional claims in published maps and institutional affiliations.



Open Access This article is licensed under a Creative Commons Attribution 4.0 International License, which permits use, sharing, adaptation, distribution and reproduction in any medium or format, as long as you give appropriate credit to the original author(s) and the source, provide a link to the Creative Commons license, and indicate if changes were made. The images or other third party material in this article are included in the article's Creative Commons license, unless indicated otherwise in a credit line to the material. If material is not included in the article's Creative Commons license and your intended use is not permitted by statutory regulation or exceeds the permitted use, you will need to obtain permission directly from the copyright holder. To view a copy of this license, visit <http://creativecommons.org/licenses/by/4.0/>.

© The Author(s) 2018